Interannual and decadal variability of the ice-shelf basal melting in the Amundsen region, West Antarctica - Focus on the oceanic factors

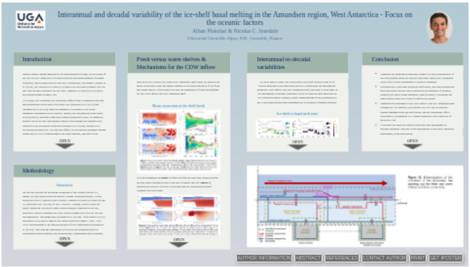
Interannual and decadal variability of the ice-shelf basal melting in the Amundsen region, West Antarctica - Focus on the oceanic factors
Alban Planchat & Nicolas C. Jourdain
Université Grenoble Alpes, IGE, Grenoble, France

Alban Planchat & Nicolas C. Jourdain

Université Grenoble Alpes, IGE, Grenoble, France

PRESENTED AT:

AGU FALL MEETING
Online Everywhere | 1–17 December 2020

INTRODUCTION

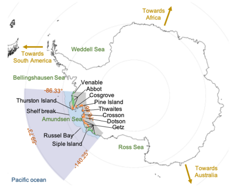

Figure 1. Studied area. The shaded zone in the western part of Antarctica corresponds to the simulated region. It covers the entire Amundsen Sea, slightly outflanking towards the Ross Sea to the west and towards the Bellingshausen Sea to the east. The limit between the deep ocean (light purple) and the shelf (light blue) is represented with a grey continuous line at the shelf break. The main ice-shelves of the region are colored either in orange for those part of the Amundsen Sea and in green for the others. In the analysis, we especially refer many times to Russel Bay, which is between roughly 128°W and 124°W at the shelf break .

Facing climate change imposed by the anthropogenic forcing, the evolution of the ice cover in Antarctica is of great interest in the understanding of climate feedbacks, and in particular sea level rise. In particular, according to Rignot et al. (2019), the Antarctic Ice Sheet (AIS) mass loss has been booming over the past four decades especially for the West Antarctic Ice Sheet (WAIS) with a non-linear increase in mass loss.

As a result, the Amundsen Sea catchment suffers from a continuous increase and intermittent acceleration of its mass loss (Dutrieux et al. (2014) and Mouginot et al. (2014)), which is assumed to be driven by the ocean variability underneath the ice-shelves. Indeed, the Circumpolar Deep Water (CDW) inflow, carrying a high heat content available for melt, is commonly pointed out as the only mechanism capable of increasing the available heat content for the ice-shelves basal melt (Thoma et al. (2008), Jenkins et al. (2018) and Holland et al. (2019)) with effects on the glaciers dynamics further inland due to a loss of buttressing at the outlet glaciers, and thus a flow acceleration of the glaciers (Mouginot et al. (2014) and Jenkins et al. (2018)). Notably, spatially coherent cool and warm periods on the shelf were observed (Mouginot et al. (2014), Dutrieux et al. (2014) and Jenkins et al. (2018)), and kept the focus of modelling studies.

On the other hand, Thompson et al. (2018) observed that the Amundsen Sea is a transition zone between a western fresh shelf and an eastern warm shelf with a blurred limit between both, questioning the impact of the (near-)circumpolar westward Antarctic Slope Current (ASC) - characteristic in the fresh shelf zone - on blocking the influence of the eastward Antarctic Circumpolar Current (ACC) - which carries the warm and salty CDW along the shelf break in a warm shelf zone.

Here, we revisit the ocean circulation at the shelf break throughout the Amundsen Sea (**Figure 1**) using a multi-decadal ocean simulation accounting for tides and ocean-ice-shelves interactions. We bring our stone to the building in the understanding of the interannual-to-decadal variability of the ice-shelves basal melt rates connecting it to the ocean fluctuations at the shelf break.

METHODOLOGY

Overview

- Present our 1/12° simulation covering the Amundsen region from 1980 to 2018 with an ocean-sea ice coupling

- Delineate the continental shelf break with accuracy and create a reference frame centered on this feature

Simulation

We use the Nucleus for European Modelling of the Ocean (NEMO-3.2, Madec (2016)) that includes the general oceanic circulation model, *Océan Parallélisé* (OPA), and the sea ice model, Louvain-la-Neuve Ice Model (LIM-3.6, (Rousset et al. (2015)), for the "AMUXL" domain, which covers the entire Amundsen Sea with a slight zonal extension compared to the one previously used in Jourdain et al. (2017) and Jourdain et al. (2019). We run this simulation - including tides (Jourdain et al. (2019)) - from March 1972 to December 2018, but we analyze the output data from January 1980 - 1972-1979 corresponding to the spin-up duration of the configuration (Jourdain et al. (2017)). This regional simulation is forced at the boundaries (sea ice concentration and thickness, and ocean salinity, temperature and velocities), and has for initial state a global simulation on the grid ORCA025. Both regional and global simulations are forced by the atmospheric reanalysis data from DFS5 (Drakkar Forcing Set) based on ERAinterim from 1979 and ERA40 before 1979. The model is run with 75 vertical levels ranging from 1m at the surface to up to 204m at 6000m, and uses the latest available Antarctic bathymetry and ice-shelves topography, BedMachine. Finally, we take advantage of an isotropic resolution of 1/12° in longitude. Please consider that such a resolution enables to correctly resolve the mean flow-topography interaction inside the submarine troughs on the shelf, but it cannot resolve the wave-topography interaction.

Shelf break reference frame

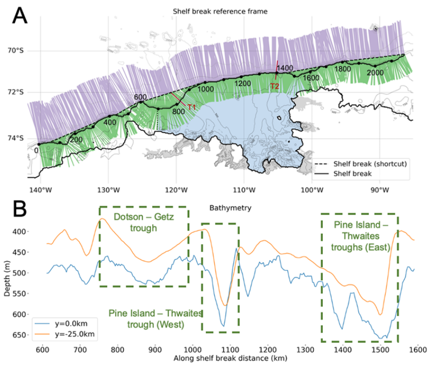

Figure 2. Change of reference frame equivalent to a juxtaposition of (near-)orthogonal transects to the shelf break. (**A**) The coastal margin and the continental shelf break are displayed with a continuous black line and the shelf break shortcut is represented with a black dashed line. Each colored line corresponds to the transect used in the reference frame we created for all the points composing the shelf break line. The green color parts refer to projections on the aligned and orthogonal normalized vectors of the shelf break line, whereas the purple ones refer to projections on the aligned and orthogonal normalized vectors of the shelf break line shortcut. The along shelf break distances - initiated at the western limit - are marked by dots every 100km. The red lines T1 and T2 are the two cross-sections used on **Figure 4**. The ice-shelves of interest are colored in grey, and finally, the blue area - delineated by the coastal margin to the south, the shelf break line to the north and the dotted lines to the west and east - is the area used **Figure 8** to average on the Amundsen shelf. (**B**) shows the bathymetry along the shelf break (blue line) and 25km further downstream onto the continental shelf (orange line). The green zones delimit the different Amundsen Sea troughs of interest commonly reported in the scientific literature for the region.

In order to highlight the processes occurring along and across the shelf break we created a reference frame centered on this feature keeping the original vertical axis. First, we delineated the shelf break with accuracy using a seabed slope gradient threshold - fit for the Amundsen Sea region - instead of using an iso-bath line. Second, on the one hand, we set the new x axis as the shelf break line, and on the other hand, we defined the new y axis as the (near-)orthogonal transects to the shelf break. We were then able to project the desired parameters in this shelf break reference frame from 100km on-shelf to 200km off-shelf (**Figure 2**). In fact, it should be considered as the juxtaposition of (near-)orthogonal transects to the shelf break. Note that we had to use a shortcut of the shelf break line, further offshore and cutting the bays encountered on its path, so as to keep this change of reference frame as meaningful as possible and avoid overlapping.

FRESH VERSUS WARM SHELVES & MECHANISMS FOR THE CDW INFLOW

Overview

- Characterize the Amundsen shelf (fresh versus warm)

- Create a Fresh-Warm Boundary Index (FWBI)

- Suggest mechanisms for the CDW inflow

Rich in a tool to watch the ocean at the Amundsen shelf break, we analyze the mean ocean state along this feature leading to the characterization of the fresh and warm shelves of the region, but also the suggestion of some mechanisms for the CDW inflow onto the Amundsen shelf.

Mean ocean state at the shelf break

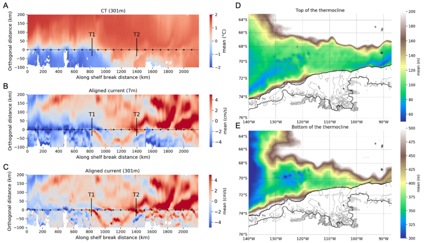

Figure 3. Mean ocean state at the shelf break. (**A**), (**B**) and (**C**) respectively show the mean CT at 301m and the mean aligned current at 7 and 301m. The black continuous line at y=0km corresponds to the shelf break with markers every 100km. The cross-sections T1 and T2 (cf. **Figure 2**) used on **Figure 4** are also drawn. (**D**) and (**E**) show the mean thermocline top and bottom depths off the Amundsen shelf, which is delineated with a black continuous line.

We can distinguish on **Figure 3** a fresh shelf in the west and a warm shelf in the east with a transition zone to the east of Russel Bay (cf. **Figure 1**), between the Dotson-Getz (Do-Ge) trough and the western Pine Island-Thwaites (Pi-Th) trough.

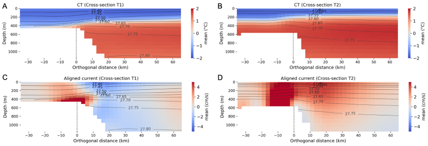

Figure 4. Cross-sections mean state. (**A**) and (**B**) (resp. (**C**) and (**D**)) are the cross-sections T1 and T2 (cf. **Figure 2**) of the CT (resp. the aligned current) for depths above 1152m and for an orthogonal distance to the shelf break between -35 and 65km. Note that for (**C**) and (**D**) a red (resp. bleu) color means that the current is globally eastward (resp. westward). T1 is used as an example of the fresh shelf cross-section in the core of the Dotson-Getz (Do-Ge) trough at x=826km and T2 is an example of the warm shelf cross-section in the core of the eastern Pine Island-Thwaites (Pi-Th) troughs (left one) at x=1398km. Iso-PDA lines are plotted every 0.05kg/m3 and the shelf break is pointed out through the dotted black line at y=0km.

Figure 4 are typical cross-sections for the fresh and warm shelves at the entry of two submarine troughs located along the shelf break. The fresh shelf is characterized by a relativeley deep thermocline at the shelf break, impeaching the CDW to lick onto the continental shelf. As opposed to the warm shelf for which the thermocline is relatively shallow enabling the warm and salty CDW to intrude onto the shelf. In addition, a westward current is present just off the shelf break in the fresh shelf zone, which corresponds to the ASC, whereas a rather barotropic eastward current flows just off the shelf break in the warm shelf zone, which corresponds to an ACC branch.

Fresh-Warm Boundary Index (FWBI)

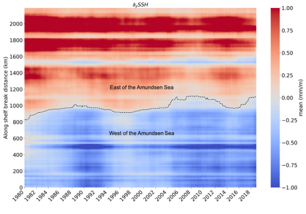

Figure 5. Fresh-Warm Boundary Index (FWBI). Hovmöller diagram - with a running mean over 5 years - of the SSH gradient orthogonal to the shelf break and averaged for y∈[0,25]km for each point along the shelf break. The dashed black line corresponds to the variability of the FWBI we suggest to delimit the fresh and warm shelves.

As we reckon that the the eastern part of Russel Bay plays a key role in the processes ruling the ocean variability in the Amundsen Sea, we took the initiative to create an index to delineate the limit between the fresh and warm shelves in the region. Moreover, the difficulty to gather *in situ* data in the region through time pushed us to think about an index, which could be followed from satellite observations. Thus, in order to put together the objective of the creation of an index with its remote sensing accessibility, we aimed at the definition of the Fresh-Warm Boundary Index (FWBI) based on the Sea Surface Height (SSH). In a word, the reversal of the surface currents between the fresh and the warm shelves (ASC versus ACC branch), is coherent with a reversal of the SSH gradient orthogonal to the shelf break. Thus, the FWBI is simply defined as the shift between a negative and a positive SSH gradient orthogonal to the shelf break. This shift is clearly apparent on the Hovmöller diagram of the SSH gradient (**Figure 5**) enabling us to draw the time series of the FWBI.

We note that such an index is particularly interesting to point out the location where the ASC seems to be initiated through time, with an outflow of water from the shelf and the initiation of easterlies at the shelf break at this limit. In short, it gives information on the ocean surface layer, which could differ from the ocean state deeper, since the transition limit between the fresh and warm shelves appear to be depth-dependent, especially when using a thermocline criterion. As a result, although the western and eastern Pi-Th troughs can be considered with confidence as part of the warm shelf zone, the Do-Ge trough characterization could be slightly more difficult. Looking at the surface layer, the Do-Ge trough is always part of the fresh shelf zone. However, things seem more complex when it comes to questioning the licking of the CDW onto the continental shelf in the eastern part of the trough. Indeed, the magnitude of the thermocline variability at the shelf break seems to be enough, in this particular zone, to make it intermittently pass in a warm shelf configuration at the shelf break even though the surface layer of the ocean appears in accordance with a fresh shelf zone.

The interannual-to-decadal variability of this index is further discuss in the next section.

Mechanisms for the CDW inflow

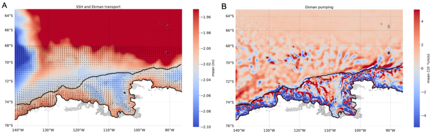

Figure 6. Effects of the top boundary of the ocean. (**A**) shows the mean SSH (slightly saturated) in our studied domain with the mean Ekman transport induced by the wind for latitudes below -68° to avoid the erasure of the specificities on the shelf and close to the shelf break with the great values encountered in the north of the studied area. (**B**) illustrates the mean Ekman pumping calculated from the ocean surface stress - induced either by the wind or the sea ice. Some white arrows are drawn in order to show the strong surface currents in a few zones of interest regarding the lid effect of sea ice, which directly influences the Ekman pumping. The coastal margin and the shelf break are represented with a continuous black line.

From the analysis of the mean ocean state at the shelf break, we suggest four different mechanisms that could play a role in the CDW inflow onto the continental shelf. First, as regularly underlined in the literature, the shift between the westerlies and the easterlies entail an Ekman pumping, which appears to be along the shelf break in the warm shelf zone whereas it is further offshore in the fresh shelf zone - due to easterlies blowing at the shelf break in the western Amundsen Sea, from Russel Bay (**Figure 6A**). Second, we question the importance of an Ekman pumping induced by sea ice (**Figure 6B**). In fact, sea ice strengthens the stress curl at the surface, with, in average, an Ekman pumping, in the area seasonally covered by sea ice strongly associated to the surface currents due to the lid effect of sea ice. It would result from the relative velocity difference between sea ice and the surface currents, and the important spatial variability of the shear stress imposed by sea ice. In is illustrated by an upwelling on the left side of a surface current and downwelling on the right side. In particular, it is observed along the shelf break with the presence of the eastward "undercurrent" - which is rather baroclinic, but still effective in the surface layer -, but also with the ASC. Then, even though we report that the bottom friction is probably partly misrepresented due to the low vertical resolution at the bottom, we can infer, all the same, a mechanism happening along the shelf break linked to the westward current flowing along the continental slope up to the continental shelf (**Figure 4C,D**). In the souther hemisphere, an anticyclonic current would entail a positive Ekman bottom friction resulting in an uplift of the CDW from the deep ocean. Finally, we would like to draw attention on the origin of the ACC branch that impacts the shelf break in the Amundsen region, yet it is of high importance, since it carries the warm and salty CDW. In particular, the combining of the ASC and the Ross Gyre cyclonic circulation to the very west of our studied domain entails a positive bump of SSH pointing towards the south at the south-east extremity of the Ross Gyre (**Figure 6A**). Such a situation seems to favor the creation of an ACC branch, of which a southern branch seems to stay relatively close to the shelf break with a great meander - due to the bathymetry - to the east of Russel Bay just before reaching the shelf break to the west of the western Pi-Th trough - as illustrated **Figure 10**. There, it could rather easily enter into the submarine trough due to the topography at this location. We also illustrate the possible effect and importance of this ACC branch showing the characteristics of the thermocline off the continental shelf in the extended Amundsen region (**Figure 3D,E**).

Please refer to **Figure 11** for an in-depth schematization of the fresh and warm shelves in the Amundsen Sea.

INTERANNUAL-TO-DECADAL VARIABILITIES

Overview

- Present the ice-shelves basal melt rates interannual-to-decadal variability

- Correlate it with the variability of key parameters on the continental shelf and at the shelf break

- Discuss the temperature and current anomalies at the shelf break

We were eager to study the ocean state at the shelf break in order to go further upstream in the analytical process to understand the mechanisms ruling the CDW inflow onto the continental shelf, and then, to shed light on the interannual-to-decadal variability of the ice-shelves basal melt rates in the Amundsen region. Indeed, a better understanding of such variability is key to assessing models and explaining the acceleration of marine glaciers.

Ice-shelves basal melt rates

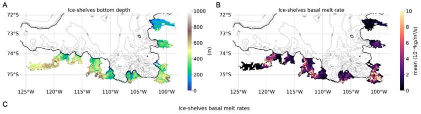

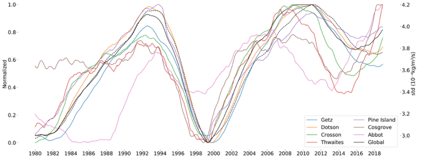

Figure 7. Ice-shelves basal melt. (**A**) and (**B**) are maps of the Amundsen shelf showing the ice-shelves bottom depth (**A**) and the mean ice-shelves basal melt rate (**B**). For each of these maps, the bathymetry is represented at 500, 750, 1,100 and 2,000m. The coastal margin and the shelf break line are displayed with a continuous line. (**C**) shows the ice-shelves basal melt rates variability between 1980 and 2018. The values for each ice-shelf are normalized between 0 and 1. The continuous black line shows the melt rate variability for all the considered ice-shelves and the dashed black line represents the associated standard deviation.

Ice-shelves have a complex topography with a large distribution of their bottom depth ranging from 0 to about 1000m in the Amundsen region (**Figure 7A**). As displayed on **Figure 7B**, most of the time, the deeper the bottom depth of the ice-shelf is, the higher the melt rate is due to the presence of CDW at depth. Not only the obtained basal melt rates underneath the ice-shelves are globally in the range of the observed values reported by Rignot et al. (2013) and Depoorter et al. (2013), but their inter annual-to-deacadal variability is also well modeled as brought out by observations-based studies (Dutrieux et al. (2014) and Jenkins et al. (2018)). Finally, we report that this variability is pretty similar for the different ice-shelves (**Figure 7C**).

Correlations

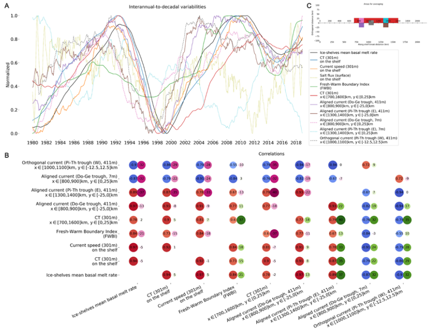

	Ice-shelves mean basal melt rate	CT (301m) on the shelf	Current speed (301m) on the shelf	Fresh-Warm Boundary Index (FWBI)	CT (301m) x∈[700,1600]km, y∈[0,25]km	Aligned current (Do-Ge trough, 411m) x∈[800,900]km, y∈[-25,0[km	Aligned current (Pi-Th trough (E), 411m) x∈[1300,1400]km, y∈[-25,0[km	Aligned current (Do-Ge trough, 7m) x∈[800,900]km, y∈[0,25]km	Orthogonal current (Pi-Th trough (W), 411m) x∈[1000,1100]km, y∈[-12.5,12.5]km
Orthogonal current (Pi-Th trough (W), 411m) x∈[1000,1100]km, y∈[-12.5,12.5]km	-0.9 -32	-0.86 -29	-0.79 -28	-0.55 -10	-0.79 -35	-0.94 -17	-0.94 0	0.72 9	
Aligned current (Do-Ge trough, 7m) x∈[800,900]km, y∈[0,25]km	-0.87 -32	-0.79 -22	-0.91 -24	-0.84 3	-0.76 -32	-0.82 -19	-0.67 -7		0.72 -9
Aligned current (Pi-Th trough (E), 411m) x∈[1300,1400]km, y∈[-25,0[km	0.89 -37	0.87 -35	0.78 -33	0.67 -13	0.79 -40	0.93 -22		-0.67 7	-0.94 0
Aligned current (Do-Ge trough, 411m) x∈[800,900]km, y∈[-25,0[km	0.97 -13	0.91 -8	0.91 -9	0.77 11	0.77 -18		0.93 22	-0.82 19	-0.94 17
CT (301m) x∈[700,1600]km, y∈[0,25]km	0.78 2	0.9 5	0.81 7	0.6 37		0.77 18	0.79 40	-0.76 32	-0.79 35
Fresh-Warm Boundary Index (FWBI)	0.84 -21	0.73 -15	0.84 -18		0.6 -37	0.77 -11	0.67 13	-0.84 -3	-0.55 10
Current speed (301m) on the shelf	0.97 -5	0.92 1		0.84 18	0.81 -7	0.91 9	0.78 33	-0.91 24	-0.79 28
CT (301m) on the shelf	0.94 -5		0.92 -1	0.73 15	0.9 -5	0.91 8	0.87 35	-0.79 22	-0.86 29
Ice-shelves mean basal melt rate		0.94 5	0.97 5	0.84 21	0.78 -2	0.97 13	0.89 37	-0.87 32	-0.9 32

Figure 8. Correlations between the ocean state, either at the shelf break or on the shelf, and the ice-shelves mean basal melt rate. On the one hand, (**A**) shows the time series with a 5-year running mean of a chosen set of parameters averaged on areas colored (with the same color as for the time series) in the shelf break reference frame on (**C**), but for the values on the shelf - which are averaged on the blue zone colored on **Figure 2**. The dashed lines refer to parameters which are anticorrelated with the ice-shelves mean basal melt rate, and were then represented as 1 – Normalized values to make the comparison more visual. On the other hand, (**B**) is a double entry table which indicates both the maximum correlation coefficient between the considered two time series and the lag (in months) associated to this correlation coefficient. The correlation coefficient is to the left with colors and sizes depending on its amplitude from blue to red. The lag is to the right with colors and sizes depending on its amplitude from pink to green. Note that for the top left triangle of the double entry table, a negative (resp. positive) lag means that the considered parameter on the horizontal is in advance (resp. delayed) compared to the one on the vertical. The two dotted lines on (**A**) are not represented in this table due to their relatively weak correlation with the ice-shelves mean basal melt rate.

We led an in tempt to correlate this mean ice-shelves basal melt rate signal with a few key parameters on the continental shelf and at the shelf break (**Figure 8**).

Qualitatively, we report that the variability of the ocean state on the continental shelf is partly correlated with the interannual-to-decadal fluctuations of the ice-shelves basal melt rates. We used the CT and current speed at 301m averaged on the shelf to highlight this. On the other hand, the surface salt flux averaged on the shelf presents a more distinct low frequency variability, being more directly influenced by the atmospheric forcing.

Then we focus on key parameters at the shelf break, and check how they are correlated with the melt activity underneath the ice-shelves. The parameters we use are averaged over different areas of interest, which are shown **Figure 8C**. Let's review the correlations associated to these parameters. We observe that the aligned current just on the shelf close to the seabed, at 411m, corresponding to the commonly called eastward "undercurrent", presents a low frequency variability which is close to the one of the ice-shelves mean basal melt rate. In particular, it seems that the fluctuations of this current at the shelf break intervene in the eastern Pi-Th trough prior to the Do-Ge trough. We also notice that the fluctuations of the orthogonal current at the entry of the western Pi-Th trough close to the seabed at 411m - corresponding to an area where the ACC branch seems to interact with the topography favoring the entry of CDW in the submarine trough - is highly anti-correlated (cf. this orthogonal current is globally southward and then negative) with the fluctuations of the eastward "undercurrent" in the eastern Pi-Th trough. This highlights the strong connection between these two troughs. In a nutshell, it seems that an increase in the entry of the CDW in the western Pi-Th is associated with an intensification of the eastward "undercurrent" in the eastern Pi-Th trough. The aligned current just off the shelf in front of the Do-Ge trough at 7m, corresponding to the ASC, is also strongly anti-correlated with the basal melt activity along the coastline (cf. this aligned current is globally westward and then negative). However, we observe that the aligned current just off the shelf in front of the eastern Pi-Th trough at 7m, corresponding to an ACC branch, has a distinct low frequency variability compared to the one of the ocean on the shelf. Surprisingly, we do not see a strong correlation between the eastward "undercurrent" in the eastern Pi-Th trough with the ACC branch just off the shelf whereas we observe a good anti-correlation between the eastward "undercurrent" in the Do-Ge trough and the ASC just off the shelf. But interestingly, we also note that the CT averaged just off the Amundsen shelf at 301m is less correlated with the ice-shelves mean basal melt rate than the different currents we discussed. However, as for the CT averaged on the shelf, we observe that its fluctuations are almost synchronised with those for the mean basal melt rate along the coastline. Finally, a word on the FWBI, which presents an important correlation even though the decrease around 2000 is less marked.

Although these correlations should be taken with a grain of salt, especially when it comes to discussing the different lags - and then causality - between the key parameters we chose, we reckon that this gives insights on the more general circulation in the Amundsen Sea and how this could have an impact on the interannual-to-decadal variability of the ice-shelves basal melt rates.

Temperature versus current anomalies

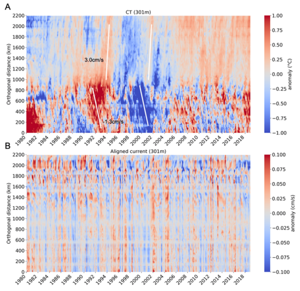

Figure 9. Variabilities at the shelf break. Hovmöller diagrams of the CT anomaly at 301m (**A**) and the aligned current at 301m (**B**) averaged between y=0 and y=25km all along the shelf break. Note that a red (resp. blue) aligned current anomaly means that the current is globally more eastward (resp. westward) compared to the mean.

A few words on the temperature and current anomalies to improve our understanding of the region. Actually, the recourse to Hovmöller diagrams is key to understand these variabilities (**Figure 9**). Especially the aligned current at the shelf break at 301m illustrates the high frequency variability of the currents at the shelf break, with almost vertical anomalies. In particular, the ASC seems to be intermittently absent along the fresh shelf zone, whereas the ACC branch is stable over time despite the anomalies. As opposed to the aligned current, the CT at 301m shows variabilities at lower frequencies. In particular, it seems that the anomalies are initiated along Russel Bay. These CT anomalies then propagates eastward to the east and westward to the west at different speeds. In particular, this highlights the importance to understand the key processes occurring in Russel Bay to shed light on the ocean state along the Amundsen shelf break, but also on the shelf itself.

CONCLUSION

Summary

- Our simulation has been validated especially thanks to a good reproduction of the observations-based ice-shelves basal melt rates in the Amundsen Sea as well as their interannual-to-decadal variability.

- The ocean state along the shelf break has been described, distinguishing the fresh and warm shelves with in particular the initiative of an index creation, the Fresh-Warm Boundary Index (FWBI), to delineate the limit between these two types of shelf in the region.

- Some mechanisms have been suggested for the CDW inflow onto the Amundsen shelf pointing out, for instance, the possible role of a sea ice induced Ekman pumping along the shelf break, and the topography effect associated to an apparent ACC branch initiated to the south-east of the Ross Gyre.

- The mean ice-shelves basal melt rate interannual-to-decadal variability has been correlated with the ocean fluctuations on the shelf, and more importantly, at the shelf break.

- Various schematizations have been shared to synthetize the large range of information we were able to derive from our simulation (**Figures 11, 12 and 13**)

To conclude, from our analysis, we infer that Russel Bay - located between the Dotson-Getz trough and the western Pine Island-Thwaites trough, in the transition zone between the fresh and warm shelves - is a critical area to study being at the jonction between what we report as core parameters in the understanding of the ocean variability driving the basal melt activity underneath the ice-shelves. These are the initiation of the ASC, the impact of the ACC branch initiated to the south-east of the Ross Gyre, and the thermocline depth along the shelf break in Russel Bay. We reckon that a sensitivity analysis of these parameters to the atmospheric forcing and the different climate modes of variability impacting the region could be key in the ongoing research aiming at including a proper ice-shelves parameterization in the Climate Model Intercomparison Project Phase 6 (CMIP6).

Paper in progress

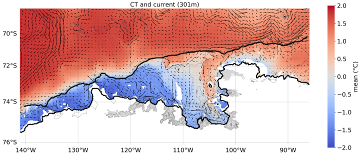

Figure 10. Zoom in on the Amundsen shelf and the continental slope to display the mean CT at 301m (colored) and the mean currents at the same depth (black arrows). The ice-shelves of interest in this study are shaded in grey whereas the others are not represented.

Fresh shelf zone
Warm shelf zone

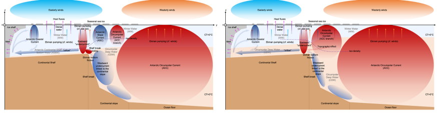
Easterly winds
Westerly winds
Heat fluxes
Seasonal sea ice
Ice shelf
Melt
Dense water
Winter Water (WW)
Antarctic Coastal Current
Ekman pumping (cf. winds)
Ekman pumping (cf. sea ice)
Antarctic Slope Current (ASC)
Antarctic Circumpolar Current (ACC branch)
Eastward "undercurrent"
Isopycnal
"Inflow"
Antarctic Continental Shelf Bottom Water (ACSBW)
Shelf break ticking
Circumpolar Deep Water (CDW)
Ekman bottom friction
Westward undercurrent linked to the continental slope
Continental Shelf
Shelf break
Continental slope
Ocean floor
Antarctic Circumpolar Current (ACC)
CT=0°C
Topography effect

Figure 11. Schematization of the ocean state across the fresh and warm shelves in the Amundsen Sea suggesting key mechanisms for the CDW inflow onto the contінetal shelf.

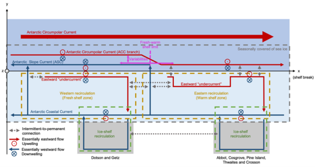
y
z
x
(shelf break)
Antarctic Circumpolar Current
Fresh-warm shelf limit
Seasonally covered of sea ice
Antarctic Circumpolar Current (ACC branch)
Variabilities
Antarctic Slope Current (ASC)
Eastward "undercurrent"
Eastward "undercurrent"
Western recirculation (Fresh shelf zone)
Eastern recirculation (Warm shelf zone)
Antarctic Coastal Current
Ice-shelf recirculation
Ice-shelf recirculation
Dotson and Getz
Abbot, Cosgrove, Pine Island, Thwaites and Crosson
Intermittent-to-permanent connection
Essentially eastward flow
Upwelling
Essentially westward flow
Downwelling

Figure 12. Schematization of the circulation in the Amundsen Sea pointing out the fresh and warm shelves and their connectivity.

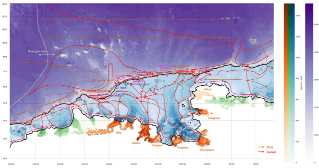

Figure 13. Global overview of the ocean state in the Amundsen Sea. It tries to summarize the ocean circulation, the winds and some particular properties of the ocean along the continental shelf break. As for **Figure 1**, the deep ocean, the shelf and both the ice-shelves of interest and the others were respectively colored in purple, blue, orange and green with an amplitude depending on the seabed depth. The coastal margin and the shelf break are also represented with continuous black lines.

AUTHOR INFORMATION

Alban Planchat, former intern at IGE (CryoDyn), Grenoble, France, working with Nicolas C. Jourdain. Currently PhD student between ENS (LMD) and UPMC (LOCEAN), Paris, France, working with Laurent Bopp and Lester Kwiatkowski in Marine Biogeochemistry on Ocean Acidification and calcifying organisms.

Nicolas Jourdain, research scientist at CNRS, studying the interactions between the Antarctic Ice Sheet and the climate system at IGE, Grenoble, France.

ABSTRACT

Following observations of a drop in the West Antarctic Ice Sheet (WAIS) mass balance over the last few decades with the possibility to reach a tipping point leading to ineluctable glaciers outlets instability in the region, understanding the driving processes has become a priority. In particular, the Circumpolar Deep Water (CDW) intrusion onto the continental shelf in the Amundsen Sea is, nowadays, in the spotlight, and gathers the attention of both the observers and the modellers. This modelling study presents the analysis of a 1/12° simulation of the Amundsen Sea sector reproducing well the interannual-to-decadal variability of the ice-shelves basal melt rates. The development of a methodology to study the ocean state in the reference frame of the continental shelf break enables us to distinguish and characterize a western fresh shelf zone and an eastern warm shelf zone in the region. Connecting it with the more regional circulation, we try to shed light on the different mechanisms driving the CDW inflow onto the continental shelf in the region. In particular, we draw attention to the sea ice effect in terms of Ekman pumping along the shelf break, and we point out the possible initiation of a southern Antarctic Circumpolar Current (ACC) branch to the south-east of the Ross Gyre, which could control part of the variability along the Amundsen Sea shelf. Finally, we discuss correlations between the ocean variability at the shelf break and the one of the melt activity underneath the ice-shelves.

REFERENCES

Rignot, E., Mouginot, J., Scheuchl, B., van den Broeke, M., van Wessem, M. J., & Morlighem, M. (2019). Four decades of Antarctic Ice Sheet mass balance from 1979–2017. Proceedings of the National Academy of Sciences, 116(4), 1095-1103.

Dutrieux, P., De Rydt, J., Jenkins, A., Holland, P. R., Ha, H. K., Lee, S. H., ... & Schröder, M. (2014). Strong sensitivity of Pine Island ice-shelf melting to climatic variability. Science, 343(6167), 174-178.

Mouginot, J., Rignot, E., & Scheuchl, B. (2014). Sustained increase in ice discharge from the Amundsen Sea Embayment, West Antarctica, from 1973 to 2013. Geophysical Research Letters, 41(5), 1576-1584.

Thoma, M., Jenkins, A., Holland, D., & Jacobs, S. (2008). Modelling circumpolar deep water intrusions on the Amundsen Sea continental shelf, Antarctica. Geophysical Research Letters, 35(18).

Jenkins, A., Shoosmith, D., Dutrieux, P., Jacobs, S., Kim, T. W., Lee, S. H., ... & Stammerjohn, S. (2018). West Antarctic Ice Sheet retreat in the Amundsen Sea driven by decadal oceanic variability. Nature Geoscience, 11(10), 733-738.

Holland, P. R., Bracegirdle, T. J., Dutrieux, P., Jenkins, A., & Steig, E. J. (2019). West Antarctic ice loss influenced by internal climate variability and anthropogenic forcing. Nature Geoscience, 12(9), 718-724.

Thompson, A. F., Stewart, A. L., Spence, P., & Heywood, K. J. (2018). The Antarctic Slope Current in a changing climate. Reviews of Geophysics, 56(4), 741-770.

Madec, G., Bourdallé-Badie, R., Bouttier, P. A., Bricaud, C., Bruciaferri, D., Calvert, D., ... & Ethé, C. (2017). NEMO ocean engine.

Rousset, C., Vancoppenolle, M., Madec, G., Fichefet, T., Flavoni, S., Barthélemy, A., ... & Vivier, F. (2015). The Louvain-La-Neuve sea ice model LIM3. 6: global and regional capabilities.

Jourdain, N. C., Mathiot, P., Merino, N., Durand, G., Le Sommer, J., Spence, P., ... & Madec, G. (2017). Ocean circulation and sea‐ice thinning induced by melting ice shelves in the A mundsen S ea. Journal of Geophysical Research: Oceans, 122(3), 2550-2573.

Jourdain, N. C., Molines, J. M., Le Sommer, J., Mathiot, P., Chanut, J., de Lavergne, C., & Madec, G. (2019). Simulating or prescribing the influence of tides on the Amundsen Sea ice shelves. Ocean Modelling, 133, 44-55.

Rignot, E., Jacobs, S., Mouginot, J., & Scheuchl, B. (2013). Ice-shelf melting around Antarctica. Science, 341(6143), 266-270.

Depoorter, M. A., Bamber, J. L., Griggs, J. A., Lenaerts, J. T., Ligtenberg, S. R., van den Broeke, M. R., & Moholdt, G. (2013). Calving fluxes and basal melt rates of Antarctic ice shelves. Nature, 502(7469), 89-92.